Mechanism and Experiment of Planar Electrode Sensors in Water Pollutant Measurement

Article *in* IEEE Transactions on Instrumentation and Measurement · February 2015

DOI: 10.1109/TIM.2014.2340641

CITATIONS
36

READS
265

6 authors, including:

Xiaolei Wang
South-Central University For Nationalities
4 PUBLICATIONS **41** CITATIONS
SEE PROFILE

Yuhao Wang
Nanchang University
82 PUBLICATIONS **384** CITATIONS
SEE PROFILE

Henry Leung
The University of Calgary
499 PUBLICATIONS **9,753** CITATIONS
SEE PROFILE

S.C. Mukhopadhyay
Macquarie University
558 PUBLICATIONS **11,071** CITATIONS
SEE PROFILE

Mechanism and Experiment of Planar Electrode Sensors in Water Pollutant Measurement

Xiaolei Wang, Yuhao Wang, *Senior Member, IEEE*, Henry Leung, *Member, IEEE*, Subhas Chandra Mukhopadhyay, *Fellow, IEEE*, Mao Tian, and Junle Zhou

***Abstract*— This paper investigates the detecting mechanism of planar electrode sensor in water pollutant detection. A system composed of electrodes, bulk media, and electrode–solution interface is built up, and the corresponding equivalent circuit containing bulk and interfacial impedances is established. The influence of each part is discussed while the impedance at interface is especially focused on. The impedance spectroscopy of the circuit is divided into three parts by the cutoff frequencies caused by interfacial and bulk impedances, and each of the frequency range can be used for the measurement of different physical quantities in water. The effect of electrode, especially the combination of interdigital and coils, is analyzed, and nine different sensors were designed and fabricated. Experiments validate the accuracy and validity of the model, and the sensor with best sensitivity is found. The stability of the planar sensor is proven in the experiment too.**

***Index Terms*— Electrodes, impedance, ions, measurement, sensitivity, water pollution.**

I. Introduction

WATER is the essence of life and an important nutrient for human, animals, plants, and environment. However, contaminated water posed a significant threat in almost every aspect in China. One of the most severe water pollution is eutrophication that is often caused by too many nutritive salts such as nitrate and phosphate. Real-time monitoring for the content level of nutritive salts is the best choice to prevent and reduce the harm, and planar electrode sensor is a promising tool for detection and measurement of ion concentration [1]–[3].

Planar electrode sensors are widely used in various fields of modern technology and engineering such as industrial areas, agriculture, and engineering/scientific applications. There are three types of sensors according to their impedance characteristics. Sensors of inductive characteristic have been used as detector for nondestructive testing of the integrity of conductive and magnetic materials [4], [5]. Another type is capacitive type that is common with interdigital electrode. This kind of sensor has many applications such as moisture content measurement in pulp, monitoring the change in impedance caused by the growth of immobilized bacteria, human health confirmation based on the content of water in human skin, humidity sensors, chemical sensor, food inspection for human safety, and estimation of material dielectric properties such as food, saxophone reed, and leather [6]–[10]. The third type is the combination of inductive and capacitive planar elements, which is categorized as a passive sensor and operates on remote query basis (wireless). An example for it is real-time monitoring of water content in civil engineering materials [11]. Although the forms may be various, the measurements are mostly concerned with parameters of electromagnetic like conductivity, permittivity, and permeability, and can finally convert to resistance, capacitance, and inductance. The nature of the output of the sensor is a great advantage for online measurement.

Although some application of planar sensor in liquid quality detection has been reported [12]–[15], problems remain. The core issue is that water environment is much more complex than previous application scenarios, and the measured impedance is concerned with not only solution conductivity or permittivity, but also some interaction at the interface of water sample and sensor. Therefore, it is necessary to analyze the impedance at interface between the liquid and solid phases, and find out the best frequency range for the measurement. This paper models the interaction between sensor and water sample, details the effect of double layer at interface, relates the involved physical quantity to equivalent circuit, and finally obtains the relationship between concentration and impedance at different frequency ranges. This paper explains the detection mechanism and can be guidance for sensor design.

The remainder of this paper is organized as follows. In Section II, the model of sensor and water sample is fully discussed, and the relationship between impedance and concentration is revealed. Nine sensors with different constructs are designed and fabricated in Section III. In Section IV, a series of experiments are conducted to verify the above theory and test the detectability of the sensors. Section V is the conclusion and future work of this paper.

Manuscript received February 10, 2014; revised June 5, 2014; accepted June 8, 2014. Date of publication July 31, 2014; date of current version December 31, 2014. This work was supported in part by the Ministry of Industry and Information Technology of Taiwan, in part by the Cooperation Plan with Foreign Technology in Jiangxi Province under Grant 20141BDH80001, in part by the National Natural Science Foundation of China under Grant 60762005, in part by the Natural Science Foundation of Jiangxi Province for Youth under Grant 2010GQS0153, and in part by the Science and Technology Foundation, Department of Education in Jiangxi Province, under Grant GJJ12006. The Associate Editor coordinating the review process was Dr. Salvatore Baglio.

X. Wang and M. Tian are with the School of Electronic Information, Wuhan University, Wuhan 430072, China (e-mail: wangxlei@whu.edu.cn).

Y. Wang and J. Zhou are with the School of Information Engineering, Nanchang University, Nanchang 330031, China.

H. Leung is with the Department of Electrical and Computer Engineering, University of Calgary, Calgary, AB T2N 1N4, Canada.

S. C. Mukhopadyay is with the School of Engineering and Advanced Technology, Massey University, Palmerston North 4474, New Zealand.

Color versions of one or more of the figures in this paper are available online at http://ieeexplore.ieee.org.

Digital Object Identifier 10.1109/TIM.2014.2340641

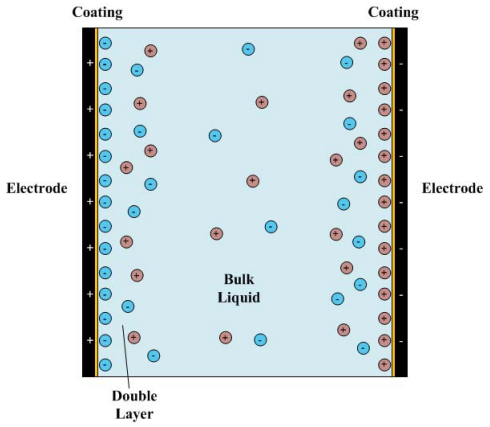

Fig. 1. Schematic diagram of water and sensor.

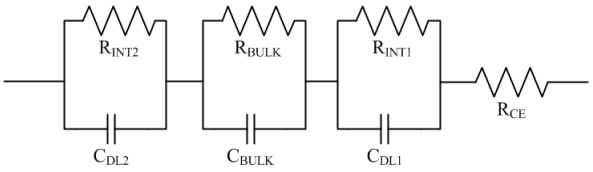

Fig. 2. Equivalent circuit of schematic diagram.

II. Detecting Mechanism and Simulation

A. Model of Electrode and Water

Unlike solid and air, liquid has its own character when the sensor is put in, and the most obvious contrast is ionic adsorption. Fig. 1 shows the schematic diagram of water sample and sensor electrodes in which adsorption effect can be distinctly observed. Charged ions are attracted at the interface between coated electrode and water solution. This phenomenon is usually called electrical double layer (EDL) [16], [17].

When a surface is immersed or created in an aqueous solution, a discontinuity is formed at the interface where such physicochemical variables as electrical potential and electrolyte concentration change significantly from the aqueous phase to another phase [18]. Because of the different chemical potentials between the two phases, charge separation often occurs at the interfacial region. This interfacial region, together with the charged surface, is usually known as the EDL, establishing a double layer capacitor. The capacitor is separated into a series of outer diffuse- and internal stern-layer capacitors. Parallel connected with the capacitor, there is an interface resistance. The resistance represents the impedance to current resulting from kinetics of specifically adsorbed or desorbed species in the electrochemical double layer.

Fig. 2 shows the equivalent circuit of schematic diagram, C_{DL1} and C_{DL2} are the double layer capacitor, R_{INT1} and R_{INT2} are the interface resistances. R_{BULK} is the resistance of solution, C_{BULK} is the capacitance of the sensor, and R_{CE} is the resistance of cable and electrode, which is mostly caused by protecting coat.

As double layer capacity can be separated into a series of diffuse- and stern-layer capacitors, the relationship between the double-, stern-, and diffuse-layer capacitances can be written in the form

$$\frac{1}{C_{\mathrm{DL}}} = \frac{1}{C_S} + \frac{1}{C_D} \tag{1}$$

where C_S has only a minimal dependency on electrolyte concentration; therefore, it is customary to assume that C_S is constant at low electrolyte concentration, which is often the case for the concentration of pollutants. On the other hand, C_D shows strong dependency on electrolyte concentration. This capacitance has a minimum value when the surface charge density is zero and increases exponentially with the surface charge density and electrolyte concentration. Thus, when concentration is low, C_S is much larger than C_D, while under high electrolyte concentration, the value of C_D is much larger than that of C_S. Because the overall capacitance is always determined by the smaller of two capacitors in series and the pollutant concentration is relatively low, C_{DL} can be equated to C_D in this case [19].

The thickness of diffuse layer can be determined from the formula for Debye length λ_{DEBYE}, which is the measure of the distance in the electrolyte over which a small potential perturbation decays by 1/e–effectively a region of space charge with an excess of charges where electroneutrality no longer holds, derived from the Poisson–Boltzmann equation [19]

$$\lambda_{\mathrm{DEBYE}} = \sqrt{\frac{\varepsilon\varepsilon_0 K_B T}{8\pi e_0^2 \Sigma z_i^2 C_i^*}}. \tag{2}$$

In (2), ε is the relative permittivity of material, ε_0 is the constant permittivity of a vacuum, K_B is the Boltzmann's constant, T is the thermodynamic temperature, e_0 is the elementary charge, z_i is the charge of species type i (number of electrons), and C^* is the concentrations of charged species. Corrected by the applied voltage V, C_D (F/cm^2) can finally be expressed as [19]

$$C_D = \frac{\varepsilon\varepsilon_0}{4\pi\lambda_{\mathrm{DEBYE}}} \cosh\frac{z_i e_0 V}{4K_B T}. \tag{3}$$

The interfacial resistance R_{INT} is predominantly caused by sorption resistance representing the impedance to current resulting from kinetics of specifically adsorbed or desorbed species in the electrochemical double layer. A derivation for electron-transfer kinetics in electroactive monolayers with an amount of adsorbed species Γ (mol/cm^2) resulted in expressions for adsorption resistance R_{ADS} as [20], [21]

$$R_{\mathrm{INT}} = R_{\mathrm{ADS}} = \frac{2R_G T}{F^2 A\Gamma k_f} \tag{4}$$

where R_G is the gas constant, T is the thermodynamic temperature, F is Faraday's constant, A is the electrode surface area, and k_f is the rate constant for the adsorption-driven kinetics. It can be inferred that when temperature is higher, interfacial resistance will increase while the double layer capacity will decrease. Therefore, the total interfacial impedance will increase as temperature rise.

To simplify the calculation of R_{BULK} and C_{BULK}, the model in Fig. 1 can be observed as a parallel plate electrode. If in a bounded sample area with the surface area of the electrodes exposed to the analyzed sample A, and thickness of the sample between the electrodes d, according to Ohm's law, the bulk media resistance is defined as

$$R_{\mathrm{BULK}} = \frac{1}{\sigma}\frac{d}{A} = \frac{d}{AF}\frac{1}{\Sigma z_i u_i C_i^*}. \tag{5}$$

The bulk resistance of a homogeneous material depends on the total conductivity σ, bulk concentration C^* of conducting species, their mobility u, charge z, sample temperature T, and the electrode geometry of the area A in which current is carried. It is worth noting that the temperature T will affect the mobility u. When T increases, the u enhance as well because the ions are easier to move in at a higher temperature. According to the definition of capacitance, C_{BULK} can be expressed as

$$C_{\mathrm{BULK}} = \frac{\varepsilon\varepsilon_0 A}{d}. \tag{6}$$

Since each part of the equivalent circuit is obtained, the total impedance of the circuit is

$$Z = R_{\mathrm{CE}} + \frac{2R_{\mathrm{INT}}}{1+\omega^2 R_{\mathrm{INT}}^2 C_{\mathrm{DL}}^2} - j\frac{2\omega R_{\mathrm{INT}}^2 C_{\mathrm{DL}}}{1+\omega^2 R_{\mathrm{INT}}^2 C_{\mathrm{DL}}^2} + \frac{R_{\mathrm{BULK}}}{1+\omega^2 R_{\mathrm{BULK}}^2 C_{\mathrm{BULK}}^2} - j\frac{\omega R_{\mathrm{BULK}}^2 C_{\mathrm{BULK}}}{1+\omega^2 R_{\mathrm{BULK}}^2 C_{\mathrm{BULK}}^2}. \tag{7}$$

Two cutoff frequencies can be defined according to the frequency spectrum characteristics of the impedance

$$f_L = \frac{1}{2\pi R_{\mathrm{INT}} C_{\mathrm{DL}}} \tag{8}$$

$$f_H = \frac{1}{2\pi R_{\mathrm{BULK}} C_{\mathrm{BULK}}} = \frac{\sigma}{2\pi\varepsilon\varepsilon_0}. \tag{9}$$

The f_L is cutoff frequency of interfacial impedance and f_H is that of solution impedance. The reason why the frequency concerned with solution is much higher than that concerned with interface is because C_{DL} is usually much larger than C_{BULK}. The cutoff frequencies are mostly used to the compare the impedance value of real and imaginary parts for both interfacial and bulk impedances. Actually the imaginary part is equated to real part when the applied frequency is the cutoff frequency. When the frequency is much lower than the cutoff frequency, the real part is much larger than imaginary part and the total impedance can be observed as a resistance. On the contrary, when the frequency is much higher than the cutoff frequency, the real part is much smaller than imaginary part and the total impedance can be observed as a capacitance. When the frequency is high enough, the total impedance is negligible, because capacitance decreases as frequency increases. When applied frequency is much lower than f_L, the impedance can be simplified as

$$Z = R_{\mathrm{CE}} + 2R_{\mathrm{INT}} + R_{\mathrm{BULK}}. \tag{10}$$

The impedance only contains resistance part, and the total resistance is the sum of coating, interfacial, and bulk resistances. As frequency increases, imaginary part is no longer insignificant and the total impedance is

$$Z = R_{\mathrm{CE}} + \frac{2R_{\mathrm{INT}}}{1+\omega^2 R_{\mathrm{INT}}^2 C_{\mathrm{DL}}^2} - j\frac{2\omega R_{\mathrm{INT}}^2 C_{\mathrm{DL}}}{1+\omega^2 R_{\mathrm{INT}}^2 C_{\mathrm{DL}}^2} + R_{\mathrm{BULK}}. \tag{11}$$

The bulk impedance is also simplified as bulk resistance, while all the imaginary part of the impedance is contributed by interfacial impedance. The significance of the expression is that it provides a method to measure the imaginary part of interfacial impedance. It is worth noting that when the frequency is f_L, the imaginary part has its maximum and the value is equated to corresponding real part of the interfacial impedance. As frequency keeps increasing, the interfacial impedance can be ignorable. When the frequency is much higher than f_L, meanwhile much lower than f_H, only water bulk and coating resistances remain, and the interfacial impedance is negligible due to the increasing of frequency

$$Z = R_{\mathrm{BULK}} + R_{\mathrm{CE}}. \tag{12}$$

Comparing (12) and (10), it is distinct that interfacial resistance can be obtained by subtraction of the resistances at two frequencies. As the coating resistance may be smaller than water bulk resistance, the total impedance dominated by only water bulk resistance, and the impedance can be simply expressed as

$$Z = R_{\mathrm{BULK}}. \tag{13}$$

This is also the frequency range for conductivity sensor measurement. When the frequency keeps increasing, the imaginary part caused by water capacitance increase and the coating resistance is no longer ignorable, so the impedance can be expressed as

$$Z = R_{\mathrm{CE}} + \frac{R_{\mathrm{BULK}}}{1+\omega^2 R_{\mathrm{BULK}}^2 C_{\mathrm{BULK}}^2} - j\frac{\omega R_{\mathrm{BULK}}^2 C_{\mathrm{BULK}}}{1+\omega^2 R_{\mathrm{BULK}}^2 C_{\mathrm{BULK}}^2}. \tag{14}$$

Finally, when frequency is much higher than f_H, the real part of water bulk impedance can be omitted

$$Z = R_{\mathrm{CE}} - j\frac{1}{\omega C_{\mathrm{BULK}}}. \tag{15}$$

In this case, the impedance shows a strong capacitive character. This frequency range is valuable in dielectric constants measurement. As the capacitive impedance decreases with an increasing frequency, it is probably that only coated electrode remains at high frequency. Considering the coating electrode, R_{CE} is set as $10^4\ \Omega$, some typical values of very low concentration solution are $R_{\mathrm{BULK}} = 10^7\ \Omega$, $C_{\mathrm{BULK}} = 10^{-10}$ F, $R_{\mathrm{INT}} = 10^6\ \Omega$, and $C_{\mathrm{DL}} = 10^{-6}$ F. According to the above equations, impedances of the 10 and 100 times concentration of the very low solution can be calculated. Fig. 3 shows the spectrum of three concentrations.

As can be observed in Fig. 3, the impedances can be divided into three parts by the two cutoff frequencies. Although the value of interfacial impedance is relatively smaller than bulk impedance, the decreasing process of interfacial impedance can be observed clearly in the figure of phase. The altering of impedance characteristic from resistance to capacitance is obvious too. As discussed above, when frequency is low enough, interfacial resistance is measurable. The imaginary part of interfacial can be better measured when the frequency is around f_L. As interfacial impedance could be a useful parameter in inorganic ions detection,

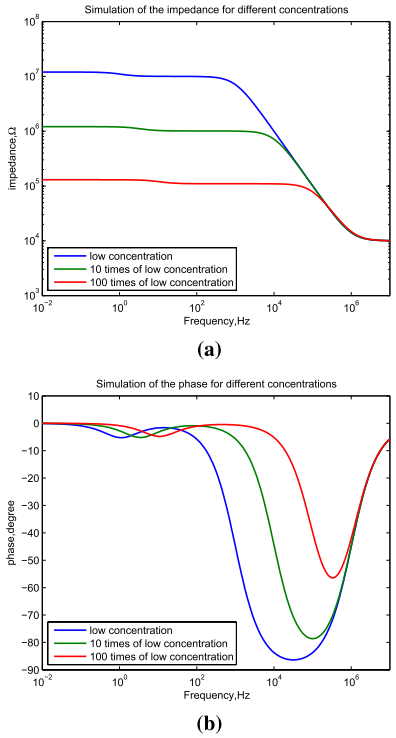

Fig. 3. Simulation of spectrum at three concentrations. (a) Simulation of impedance. (b) Simulation of phase.

the measurement is significant. The frequency between f_L and f_H, especially when frequency is much higher than f_L and much lower than f_H, is suitable for material conductivity σ and concentration of conducting species C^*. The ε can be calculated at frequency above f_H. The influence of concentration is distinct, too. The impedance and at higher concentration is evidently smaller than that of lower concentration, while the cutoff frequencies of higher concentration is higher than that of lower concentration. The differences are mainly caused by larger resistor in purer water.

B. Effect of Electrode Model

The previous section discusses the interaction between water bulk and electrode, and Fig. 3 reveals the relationship between concentration, frequency, and impedance. However, all the calculations above are based on the assumption of parallel plate electrode, which is not the case for planar electrode sensor. Although, the simplified mode as parallel plate electrode is significant in investigating the interaction between electrode and solution, the shape and form of electrode should never be negligible. Unlike the equipotent structure of parallel plate electrode, the shape of planar electrode can be unequal, so the equivalent capacitance and equivalent resistance may not follow the formulas above. Even though the equivalent structure as the parallel connection of resistance and capacitance do not change, the value of each part and the cutoff frequency as their function will certainly alter according to the shape and geometric parameters of planar electrode. For instance, although the exact relationship between water bulk resistance and dimension parameter may be different from the above equations, increasing distance between the two electrodes will obviously add the resistance, while increasing area of electrode will decrease the resistance. Thus, the total impedance may be too high to measure caused by an abnormally wide distance between the electrodes. On the other hand, unlike water bulk impedance, the equations of interfacial impedance will be less affected by unequal electrodes, because the interfacial impedance is only concerned with interfacial between water and electrode.

In addition to size and shape, potential inductance is another influence factor caused by electrode model. Coil structure, as an inductive part, is commonly used in planar sensor. Obviously, it may weaken the capacitance and change the impedance from capacitive to inductive when the frequency is high enough. The significance of coils structure is that the weakening of capacitance may help enhance measurement accuracy in some cases. For example, when water bulk is to be measured, the capacitive part of impedance will certainly interfere with measuring precision. Therefore, the use of coils in this situation will increase accuracy. Another effect of employing coils is that decrease of total impedance by weakening capacitance will increase measuring current thus reduce the measuring error. Therefore, it is meaningful to compare the electrode with coils and electrode without coils in the experiment.

Briefly, electrode model plays a critical role in sensor performance. Different structures and physical dimensions will affect the impedance to a large extent. Considering the impedance spectrum simulation, the sensor model will determine impedance spectrum for each sensor. Therefore, the detectability varies according to sensor model. In the following section, plenty of sensor models will be designed and compared.

III. Sensors Design and Measurement

A. Sensor Design

As analyzed above, the electrode model is closely concerned to sensor performance. The effect of different structures is mostly emphasized here. That is because although the geometrical parameter is matter with sensor performance, it is predictable to some extent. It is reasonable to infer that the impedance increase with corresponding distance between the electrodes and decrease with corresponding area between the electrodes. However, the effect of various electrode structures, such as different electrode shapes and coils, are more complicated. Additionally, it is easier to evaluate the effect of geometrical parameter when the effect of electrode structure is acknowledged.

The design of the sensor is based on interdigital electrode, which is the most common electrode structure for planar sensors. In addition to the traditional interdigital electrode, two modified types of interdigital electrodes, two-sided and hooked interdigital electrodes are designed for compare. Two types of coil structure, named as unilateral and bilateral coils, are also considered for evaluating the effect of inductance. Therefore, there are totally nine of the sensor shapes (Fig. 4). The top three electrodes are traditional interdigital electrode, two-sided and hooked interdigital electrodes. In the middle

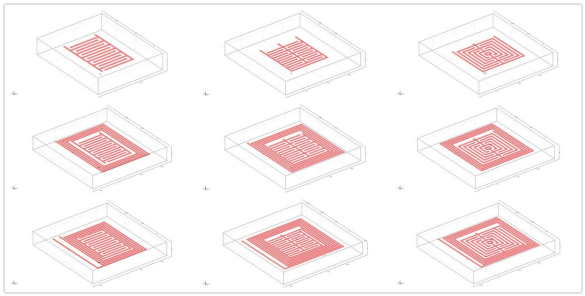

Fig. 4. Electrode design.

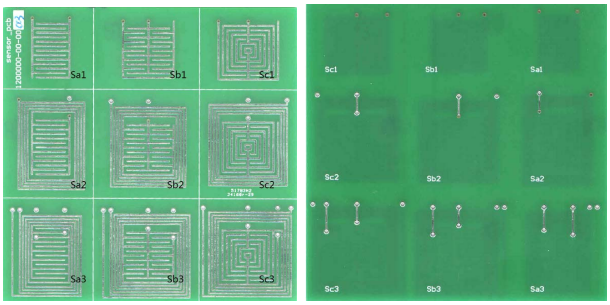

(a) (b)

Fig. 5. Top and bottom layers of the planar electrode sensor. (a) Top layer. (b) Bottom layer.

row, unilateral coils structures are added while keeping the same electrodes as the top structure. On the bottom, bilateral coils are added, keeping the same electrodes as the above.

Fig. 5 shows the fabricated sensors. Sa, Sb, and Sc represent different kinds of interdigital electrodes, and the following numbers indicate the coils types. The sensors are fabricated by printed circuit board technology with whole board size of 99 mm × 99 mm × 1.6 mm. Stannum is used to cover copper track for protection. The thickness of copper and stannum are 35 and 20 μm. The widths of electrode and pitch distances are equal to 0.5 mm. All the sensors are coated with silicon rubber to form a coating layer to prevent any direct contact with water sample.

B. Measurement Method

The sensor can be simply observed as a black box consisted of real and imaginary parts in the measurement. As the previous analysis, both real and imaginary parts are the function of the frequency applied and water sample concentration. The electrical equivalent circuit of the measurement is shown in Fig. 6.

The sensor is connected to a function generator, where R_g is the output resistance with nominal value of 50 Ω, R_r denotes the reference resistor connected to the sensor, which is used for current and phase measurements. Hence, the current I through the sensor and reference resistor, and the total impedance Z_{total} including Z_s and R_r is given by

$$I = \frac{V_2 \angle 0}{R_r} \tag{16}$$

$$Z_{\text{total}} = \frac{V_1 \angle \theta}{I} = \frac{V_1 \angle \theta}{V_2 \angle 0} R_r \tag{17}$$

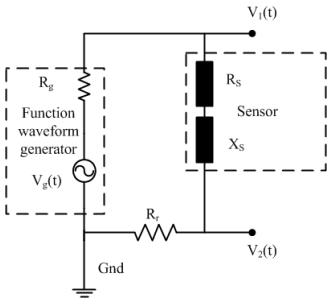

Fig. 6. Electrical equivalent circuit of the measurement of the sensor.

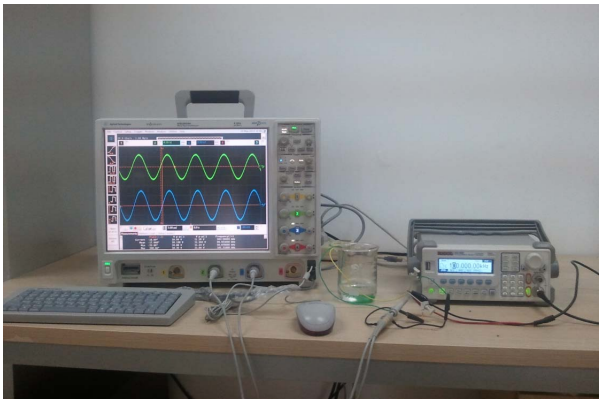

Fig. 7. Setting of the experiments.

where θ is the phase difference between $V_1(t)$ with $V_2(t)$ in degree, taking $V_2(t)$ as reference. Therefore, real part R_s, imaginary part X_s, total impedance Z_s, and phase θ_s are given by

$$R_s = Z_{\text{total}} \cos\theta - R_r \tag{18}$$

$$X_s = Z_{\text{total}} \sin\theta \tag{19}$$

$$Z_s = \sqrt{R_s^2 + X_s^2} \tag{20}$$

$$\theta_s = \text{atan}\frac{X_s}{R_s}. \tag{21}$$

The experimental setting is shown in Fig. 7. A function waveform generator, Rigol DG1022, was used to create standard sinusoidal waveform with the peak-to-peak value of 10 V as the input signal for the sensors. A 10-kΩ resistor with tolerance of 1% was used as reference resistor. A beaker was used for the sample container and the sensor was immersed into the water sample. The Agilent 9404 A mixed signal oscilloscope was used to record the output signals. The impedance of absolute value, real part, imaginary part, and phase can be calculated by (18)–(21).

IV. Experimental Characteristic of the Sensors

A. Compare of Sensors

The nine sensors were first tested in water sample with nitrate of 10 mg/L and the frequency range was 20 Hz–5 MHz. The frequency range is set according to sensor response. When the frequency is below 20 Hz, the current is too weak due to high impedance, and oscilloscope can hardly measure the precise voltage. When the frequency is above 5 MHz,

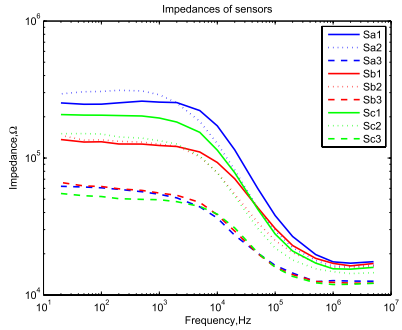

(a)

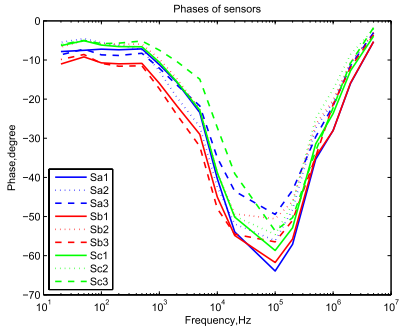

(b)

Fig. 8. Experiments for comparing the nine sensors. (a) Comparing of impedances. (b) Comparing of phases.

the impedance of sensor is stable. The aim of this experiment was to verify the theoretical analysis in Section II and compare the impedances of different sensors. As all the sensors were tested in the same solution, models of electrodes were only difference between them. Fig. 8 shows the impedance and phase for each sensor. It is apparent that the values of impedance are different while they keep almost the same tendency.

The impedance is can be divided into three stages according to the experiment result. When frequency is below 10^3 Hz, the impedance is relative stable. The impedance decreases dramatically as frequency increase when frequency is between 10^3 and 10^6 Hz. Finally, when frequency is above 10^6 Hz, the impedance is stable again although the value is much smaller than that below 10^3 Hz. The figure of phase is accordant with impedance, it shows a stronger capacitive characteristic between 10^3 and 10^6 Hz, and shows a resistive characteristic when the frequency below 10^3 Hz and above 10^6 Hz.

The low cutoff frequency are not distinct in the figures, probably illustrating that f_L is below or just around 20 Hz. On the other hand, f_H is much clearer, although there are some slightly differences, the f_H are around 10^5 Hz, illustrating that the shift of cutoff frequency caused by electrode model is mild. That is because all the sensors shared the same geometric parameters like metal thickness, electrode width, and pith distance.

It is also obvious that impedances of Sa3, Sb3, and Sc3 are smaller than others. As the three share the same bilateral coils, it can be infer that bilateral coils decrease impedance, especially water bulk resistance between the electrodes. Explanation is that the bilateral coils actually extend the area between the electrodes by surrounding each other. The same interpretation can explain why Sa1 and Sa2 have larger impedance.

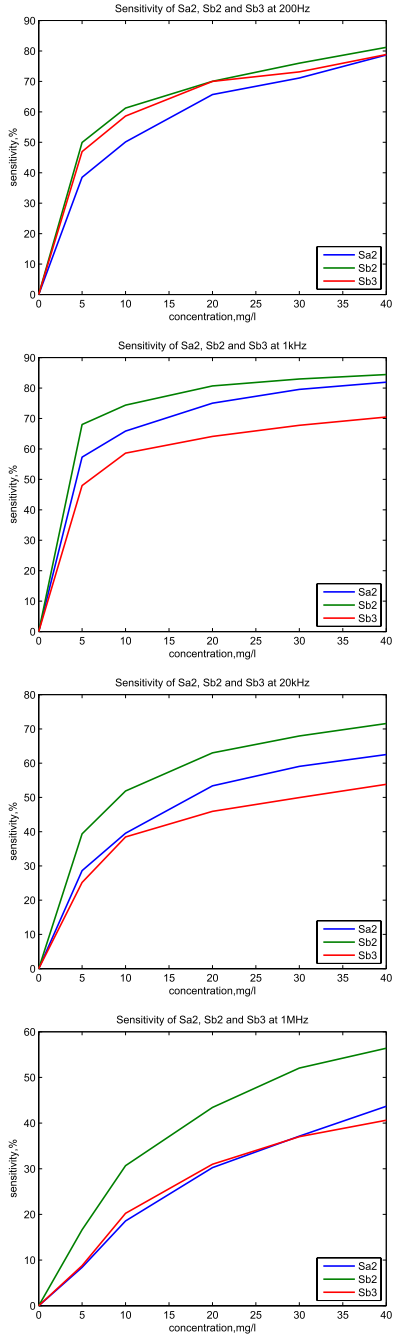

Fig. 9. Experiments for sensitivity of Sa2, Sb2, and Sb3.

As a whole, the curves in Fig. 8 confirm the simulation in Section II and prove the effect of electrodes. However, the detectabilities of the sensors are still inconspicuous, so an experiment for different concentrations is to be conducted.

B. Quantitative Experiment for Detecting Nitrate

Quantitative experiment aims at testing the response of the sensors with different concentration of nitrates samples and the sensor with best detectability will be found. The operating frequency for sensors is set at some frequencies. Sensitivity is used for evaluating the effect of the samples, and can be

calculated from the following:

$$S_{\text{impedance}} = \frac{|Z_{\text{sample}} - Z_{\text{distilled}}|}{Z_{\text{distilled}}} \times 100\% \qquad (22)$$

where Z_{sample} is the impedance of in tested sample and $Z_{\text{distilled}}$ is the impedance in distilled water as a reference. As too many curves will make the figure confusion, only sensitivity of the best threes sensors are shown in Fig. 9 and four frequencies are shown here. Sb2 is distinctly superior to Sa2 and Sb3 in terms of sensitivity, while all the three have the same trend. It is not a surprising to find out that the best three sensors has some common. Sa2 and Sb2 share the same coils type while Sb2 and Sc3 have the same interdigital part. Therefore, it can be inferred that the electrode as series connection of two-sided interdigital part and one side coils has the best detection capability. The explanation for sensitivity could be that two-sided interdigital electrode is more efficient structure and unilateral coils can help enhance measurement precision without weakening water impedance between electrodes. Therefore, the impedance measured by Sb2 is more sensitive to ions in water.

C. Performance Test of Sb2

As Sb2 had a better sensitivity than others, it was selected for more tests. As a comparison of the simulation, three water samples with nitrate concentrations of 1, 10, and 100 mg/L were prepared, so the ratio of the concentration was exactly the same with that in the simulation. This experiment was designed to observe the relationship between impedance and concentration and the difference between experiment and simulation. The frequency range was from 20 Hz to 5 MHz, and the result is shown in Fig. 10.

The difference of impedance for each concentration is distinct. Comparing with Fig. 3, it is obvious that experiment and simulation are similar in trend while some specific values are not exactly the same. The similarity of the two can confirm working principle and detecting mechanism again. The following reasons may account for the differences. First, the simulation is based on some normal values, which may not be the same as the values in experiments. Second, the frequency range of the experiment is limited, so impedances at the low frequencies are not fully presented. In addition, the difference of amplitude from 10 to 100 mg/L is smaller than that from 1 to 10 mg/L, which reveals the effect of increasing concentration is weakened for higher concentrations. Therefore, the formulas concerned with concentrations may need modification when concentration varies greatly. Measurement errors are mainly caused by temperature, jitter signal source, limited frequency range, and frequency step. As temperature and voltage are directly concerned with impedance according to the formulas in Section II, the inequality of temperature and voltage will certainly affect the impedance. Limited frequency range and frequency step may make the experiment result less smooth than the simulation result. As stability is a key performance of the sensor, Sb2 were put in the same water samples for an hour at the frequency of 2 KHz, and the impedance can be observed in Fig. 11. It is clear that the

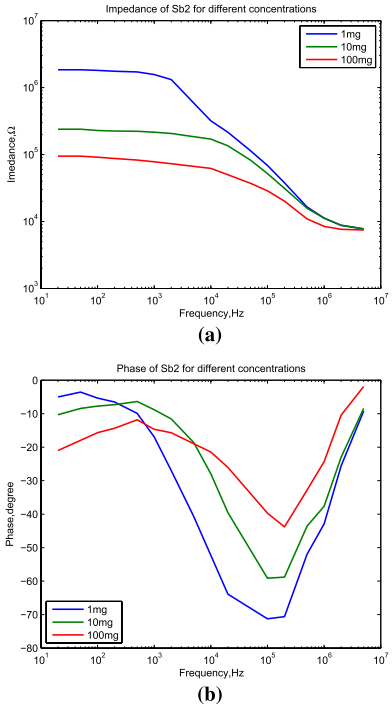

Fig. 10. Experiments for impedance spectroscopy of Sb2 in water samples. (a) Amplitude of the impedance. (b) Phase of the impedance.

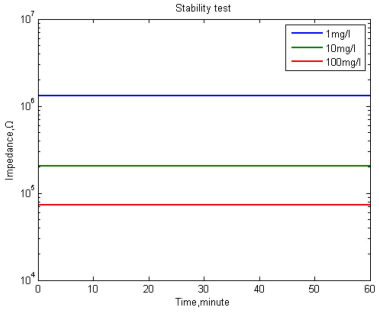

Fig. 11. Stability test of Sb2.

sensor has great stability, and experiment results also show the relative deviation are below 1%.

V. Conclusion

Planar electrode sensor is a great tool in real-time measurement for water pollutant. For investigating the working principle of the sensor, this paper model the system composed of the sensor and water sample, analyze the influencing factors of the sensor measurement. The detectability of the sensor is testified in both theory and experiment. The electrode shape with best sensitivity is picked out, and the stability is proven too. In the future, more sensors with different geometrical parameters will be designed and fabricated. The sensor will be used to distinguish inorganic type with conductivity sensor. Low-cost peripheral circuit will be built so that the sensor can be a part of portable water sensing devise or have a universal communication interface for real-time monitoring.

References

[1] C. J. Schuster-Wallace, V. I. Grover, Z. Adeel, U. Confalonieri, and S. Elliott, *Safe Water as the Key to Global Health*. Tokyo, Japan: United Nations Univ., 2008, pp. 4–7.

[2] Y. Li and K. Migliaccio, *Water Quality Concepts, Sampling, and Analyses*. New York, NY, USA: Taylor & Francis, 2011, p. 113.
[3] R. Colin and P. Quevauiller, *Monitoring of Water Quality*. Amsterdam, The Netherlands: Elsevier, 2009, pp. 26–29.
[4] D. Schlicker, A. Washabaugh, I. Shay, and N. Goldfine, "Inductive and capacitive array imaging of buried objects," *Insight, Non-Destruct. Testing Condition Monitor.*, vol. 48, no. 5, pp. 302–306, May 2006.
[5] B. George, H. Zangl, T. Bretterklieber, and G. Brasseur, "A combined inductive-capacitive proximity sensor and its application to seat occupancy sensing," in *Proc. IEEE Int. Instrum. Meas. Technol. Conf. (I2MTC)*, Singapore, May 2009, pp. 13–17.
[6] A. V. Mamishev, K. Sundara-Rajan, F. Yang, Y. Du, and M. Zahn, "Interdigital sensors and transducers," *Proc. IEEE*, vol. 92, no. 5, pp. 808–845, May 2004.
[7] A. Guadarrama-Santana and A. Garcia-Valenzuela, "Principles and methodology for the simultaneous determination of thickness and dielectric constant of coatings with capacitance measurements," *IEEE Trans. Instrum. Meas.*, vol. 56, no. 1, pp. 107–112, Feb. 2007.
[8] N. Kirchner, D. Hordern, D. Liu, and G. Dissanayake, "Capacitive sensor for object ranging and material type identification," *Sens. Actuators A, Phys.*, vol. 148, no. 1, pp. 96–104, Nov. 2008.
[9] C.-L. Zhao, M. Qin, and Q.-A. Huang, "A fully packaged CMOS interdigital capacitive humidity sensor with polysilicon heaters," *IEEE Sensors J.*, vol. 11, no. 11, pp. 2986–2992, Nov. 2011.
[10] S. C. Mukhopadhyay, J. D. Woolley, G. Sen Gupta, and S. N. Demidenko, "Saxophone reed inspection employing planar electromagnetic sensors," *IEEE Trans. Instrum. Meas.*, vol. 56, no. 6, pp. 2492–2503, Dec. 2007.
[11] J. B. Ong, Z. You, J. Mills-Beale, E. L. Tan, B. D. Pereles, and K. G. Ong, "A wireless, passive embedded sensor for real-time monitoring of water content in civil engineering materials," *IEEE Sensors J.*, vol. 8, no. 12, pp. 2053–2058, Dec. 2008.
[12] S. Bhadra, G. E. Bridges, D. J. Thomson, and M. S. Freund, "Electrode potential-based coupled coil sensor for remote pH monitoring," *IEEE Sensors J.*, vol. 11, no. 11, pp. 2813–2819, Nov. 2011.
[13] M. A. M. Yunus and S. C. Mukhopadhyay, "Novel planar electromagnetic sensors for detection of nitrates and contamination in natural water sources," *IEEE Sensors J.*, vol. 11, no. 6, pp. 1440–1447, Jun. 2011.
[14] M. A. M. Yunus and S. C. Mukhopadhyay, "Development of planar electromagnetic sensors for measurement and monitoring of environmental parameters," *Meas. Sci. Technol.*, vol. 22, no. 2, p. 025107, 2011.
[15] S. C. Mukhopadhyay, C. P. Gooneratne, G. Sen Gupta, and S. N. Demidenko, "A low-cost sensing system for quality monitoring of dairy products," *IEEE Trans. Instrum. Meas.*, vol. 55, no. 4, pp. 1331–1338, Aug. 2006.
[16] P. Delahay, *Double Layer and Electrode Kinetics*. New York, NY, USA: Interscience, 1965, p. 33.
[17] D. C. Grahame, "The electrical double layer and the theory of electrocapillarity," *Chem. Rev.*, vol. 41, no. 3, pp. 441–501, 1947.
[18] N. Singh, "Double layer formation," *Plasma Phys.*, vol. 24, no. 6, p. 639, 1982.
[19] V. F. Lvovich, *Impedance Spectroscopy: Applications to Electrochemical and Dielectric Phenomena*. New York, NY, USA: Wiley, 2012.
[20] V. F. Lvovich and M. F. Smiechowski, "Non-linear impedance analysis of industrial lubricants," *Electrochim. Acta*, vol. 53, no. 25, pp. 7375–7385, 2008.
[21] K. Darowicki and P. Ślepski, "Dynamic electrochemical impedance spectroscopy of the first order electrode reaction," *J. Electroanal. Chem.*, vol. 547, pp. 1–8, Apr. 2003.

Xiaolei Wang was born in Hubei, China, in 1984. He received the B.S. degree from the Huazhong University of Science and Technology, Wuhan, China, in 2007, and the M.S. degree from the Chongqing University of Post and Telecommunications, Chongqing, China, in 2011. He is currently pursuing the Ph.D. degree from Wuhan University, Wuhan.

His current research interests include novel sensor design, signal process, environment monitoring, and wireless sensor network.

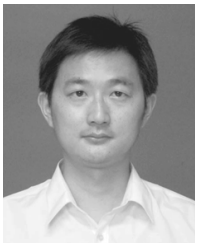

Yuhao Wang (SM'14) was born in Hubei, China, in 1977. He received the Ph.D. degree in space physics from Wuhan University, Wuhan, China, in 2006.

He was a Visiting Professor with the Department of Electrical Communication Engineering, University of Calgary, Calgary, AB, Canada, in 2008, and the China National Mobile Communication Research Laboratory, Southeast University, Nanjing, China, from 2010 to 2011. He is currently a Professor with the Cognition Sensor Network Laboratory, School of Information Engineering, Nanchang University, Nanchang, China. His current research interests include radio measurement and channel modeling, software-defined radio, complex environment sensing and monitoring, nonlinear signal processing, multimedia, sensor networks, and wireless communications.

Henry Leung (M'90) received the Ph.D. degree in electrical and computer engineering from McMaster University, Hamilton, ON, Canada.

He was with the Defense Research Establishment Ottawa, Ottawa, ON, Canada, where he was involved in the design of automated systems for air and maritime multisensor surveillance. He is currently a Professor with the Department of Electrical and Computer Engineering, University of Calgary, Calgary, AB, Canada. His current research interests include chaos, computational intelligence, data mining, information fusion, nonlinear signal processing, multimedia, sensor networks, and wireless communications.

Subhas Chandra Mukhopadhyay (F'11) received the Degree with a Gold medal from the Department of Electrical Engineering, Jadavpur University, Kolkata, India, in 1987, the M.E. degree in electrical engineering from the Indian Institute of Science, Bangalore, India, in 1989, the Ph.D. (Eng.) degree from Jadavpur University, Kolkata, India, in 1994, and the Dr.Eng. degree from Kanazawa University, Kanazawa, Japan, in 2000.

He is currently an Associate Professor with the School of Engineering and Advanced Technology, Massey University, Palmerston North, New Zealand. He has over 21 years of teaching and research experiences. He has authored and co-authored over 240 papers in different international journals, conferences, and book chapters. He has edited nine conference proceedings, also edited eight special issues of international journals as a lead Guest Editor, and 10 books out of which eight are with Springer-Verlag. His current research interests include sensors and sensing technology, electromagnetics, control, electrical machines, and numerical field calculation.

Mao Tian received the Ph.D. degree from Wuhan University, Wuhan, China, in 1988.

He is currently a Professor with the School of Electronic Information, Wuhan University. His current research interests include wireless communication, radar, and wireless sensor network.

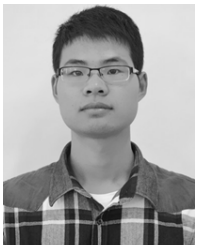

Junle Zhou was born in Jiangxi, China, in 1991. He received the B.S. degree from Nanchang University, Nanchang, China, in 2014.

His current research interests include planar electrode sensor and broadband wireless communication system.